

IMAGINE: Intelligent Multi-Agent Godot-based Indoor Networked Exploration

Tiago Leite^{a,*}, Maria Inês Conceição^{a,b,c}, António Grilo^a

^a INESC INOV, Instituto Superior Técnico, Universidade de Lisboa, Lisbon, 1000-029, Portugal

^b INESC ID-Instituto de Engenharia de Sistemas e Computadores: Investigação e Desenvolvimento, Instituto Superior Técnico, Lisbon, 1000-029, Portugal

^c Institute for Systems and Robotics, Instituto Superior Técnico, Universidade de Lisboa, Lisbon, 1049-001, Portugal

Abstract

The exploration of unknown, Global Navigation Satellite System (GNSS) denied environments by an autonomous communication-aware and collaborative group of Unmanned Aerial Vehicles (UAVs) presents significant challenges in coordination, perception, and decentralized decision-making. This paper implements Multi-Agent Reinforcement Learning (MARL) to address these challenges in a 2D indoor environment, using high-fidelity game-engine simulations (Godot) and continuous action spaces. Policy training aims to achieve emergent collaborative behaviours and decision-making under uncertainty using Network-Distributed Partially Observable Markov Decision Processes (ND-POMDPs). Each UAV is equipped with a Light Detection and Ranging (LiDAR) sensor and can share data (sensor measurements and a local occupancy map) with neighbouring agents. Inter-agent communication constraints include limited range, bandwidth and latency. Extensive ablation studies evaluated MARL training paradigms, reward function, communication system, neural network (NN) architecture, memory mechanisms, and POMDP formulations. This work jointly addresses several key limitations in prior research, namely reliance on discrete actions, single-agent or centralized formulations, assumptions of *a priori* knowledge and permanent connectivity, inability to handle dynamic obstacles, short planning horizons and architectural complexity in Recurrent NNs/Transformers. Results show that the scalable training paradigm, combined with a simplified architecture, enables rapid autonomous exploration of an indoor area. The implementation of Curriculum-Learning (five increasingly complex levels) also enabled faster, more robust training. Area coverage surpassed 95% in three levels, and the implementation of Convolutional NNs (CNNs) increased system performance by 20%. This combination of high-fidelity simulation, MARL formulation, and computational efficiency establishes a strong foundation for deploying learned cooperative strategies in physical robotic systems.

Keywords:

Multi Agent Reinforcement Learning, Godot, Autonomous Exploration, Unknown Environments, Curriculum-Learning

1. Introduction

Initially developed for military purposes, Unmanned Aerial Vehicles (UAVs) have now become increasingly popular in a wide range of applications, including commercial use, security [1], surveillance [2], cinema [3], agriculture [4], disaster management [5], and personal use [6].

The deployment of UAV teams has gained attention recently, with collaboration among UAVs being a highly desirable, albeit challenging, capability. This is inspired by natural systems where cooperation and decentralization are essential for solving complex tasks.

This work is positioned within the context of utilizing swarms of robots, particularly UAVs and potentially Micro Aerial Vehi-

cles (MAVs), for indoor exploration.

Specifically, the problem formulation is using multiple decentralized agents to explore an *a priori* unknown indoor 2D environment, whilst being able to communicate amongst themselves, given realistic network constraints.

The problem of cooperative multi-agent exploration is challenging due to environmental uncertainty and communication constraints. A comparative summary of the most relevant related works is provided in Table 1. Methodological paradigms offer distinct trade-offs. **Frontier-based** methods direct agents to unknown region boundaries [7] and use map-sharing for coordination [8, 9, 10], but can be myopic. **Planning-based** approaches use cellular decomposition [11, 12, 13] for systematic coverage, requiring a global model. **Sampling-based** algorithms like Rapidly-exploring Random Tree (RRT) [14, 15] explore complex spaces but share a high communication burden.

RL-based methods learn exploration policies, either in a two-

*Corresponding author.

Email addresses: tiagomleite@tecnico.ulisboa.pt (Tiago Leite), ines.conceicao@tecnico.ulisboa.pt (Maria Inês Conceição), antonio.grilo@inov.pt (António Grilo)

stage manner with classical planners [16] or end-to-end [17, 18]. However, Multi-Agent Reinforcement Learning (MARL) introduces coordination challenges, often addressed with computationally expensive techniques [19, 20, 21]. A significant gap remains for communication-efficient, multi-agent strategies under full uncertainty.

This work integrates in a single framework several aspects already present in the state-of-the-art, which can be considered a contribution:

- (1) Adopting the separation of concerns into mapping and decision-making, as demonstrated in [8].
- (2) Leveraging coordination mechanisms at the map level, inspired by [10], and with sensor information as in [20, 21], thereby avoiding reliance on computationally expensive techniques.
- (3) Building upon the end-to-end Deep Reinforcement Learning (DRL) paradigm and extend it to the multi-agent domain, employing a continuous action space as in [18], unlike the discrete space in [17].
- (4) Integrating strategies from [17, 18] in reward formulation.

Nevertheless, it also brings new contributions:

- (1) It adopts a MARL paradigm for UAV swarm coordination in exploration missions, addressing this current gap in the literature.
- (2) It assesses the impact of communications in mission coordination by implementing a more realistic communication model, including data rate and range limitations.
- (3) Instead of defaulting to Recurrent Neural Networks (RNNs) for partial observability, this work successfully employs a Belief-Markov Decision Process (MDP) formulation, providing a more structured and effective approach to state estimation.
- (4) It strives to keep physical realism (while also maintaining computational efficiency) by simulating the environment using the open-source game engine Godot [22], which, to the best of the authors' knowledge, is the first time this engine is applied in this field. Godot provides a lightweight, open-source platform for high-fidelity, game-engine-quality simulation, complete with physically accurate collisions for both static and dynamic objects.
- (5) Utilizing industry-grade tools (Ray/RLLib, WandB), with validation on an High-Performance Computing (HPC) cluster, ensuring reproducibility and scalability.

The remainder of this document is structured as follows. Section 2 covers the theoretical background on Network Distributed POMDP (ND-POMDP). Section 3 describes the proposed method and its practical implementation. Section 4

presents the experimental results. Finally, Section 5 presents the main conclusions and directions for future work.

2. Network Distributed-Partially Observable Markov Decision Process

The standard MARL Mathematical framework is the Decentralized Partially Observable Markov Decision Process (Dec-POMDP), defined by the tuple $(\mathcal{N}, \mathbb{S}, \mathbb{A}, \mathbb{O}, \mathcal{O}, \mathcal{T}, \mathcal{R}, \gamma)$. The Dec-POMDP can be further extended to an ND-POMDP by modeling communication constraints between agents using a graph \mathbb{G} . Therefore, an ND-POMDP is defined by the tuple $(\mathcal{N}, \mathbb{S}, \mathbb{A}, \mathcal{T}, \mathcal{R}, \mathbb{O}, \mathcal{O}, \mathbb{G}, \gamma)$:

- \mathcal{N} is the set of agents, indexed by $i \in \mathcal{N}$ where the total number of agents is $n = |\mathcal{N}|$.
- \mathbb{S} is the state space, the set of possible states.
- \mathbb{A} , where \mathbb{A}_i is the set of actions available to agent i which can be different for each agent, and $\mathbb{A} = \mathbb{A}_1 \times \mathbb{A}_2 \times \cdots \times \mathbb{A}_{|\mathcal{N}|}$ is the joint action space. At each time step t , each agent i takes an action¹ a_i^t , leading to one joint action $a = (a_1, \dots, a_{|\mathcal{N}|})$ at each time step [23].
- $\mathcal{T} : \mathbb{S} \times \mathbb{S} \times \mathbb{A} \rightarrow \mathbb{R}$ is the state transition probability function $\mathcal{T}(s', s, a) = P(s'|s, a)$, describing the probability of transitioning to state s' given current state s and joint action $a = (a_1, a_2, \dots, a_n)$.
- $\mathcal{R} : \mathbb{S} \times \mathbb{A} \rightarrow \mathbb{R}$ is the shared reward function $\mathcal{R}(s, a, s')$, providing the same scalar reward to all agents based on the current state s , joint action a and the environment transitioning to state s' .
- \mathbb{O} , where \mathbb{O}_i is the set of observations available to agent i which can be different for each agent, and $\mathbb{O} = \mathbb{O}_1 \times \mathbb{O}_2 \times \cdots \times \mathbb{O}_{|\mathcal{N}|}$ is the joint observation space.
- $\mathcal{O} : \mathbb{O} \times \mathbb{S} \times \mathbb{A} \rightarrow \mathbb{R}$ is the joint observation probability function $\mathcal{O}(o, s', a) = P(o|s', a)$, describing the probability of observing $o = (o_1, o_2, \dots, o_{|\mathcal{N}|})$ given the next state s' and joint action a .
- \mathbb{G} : The set of all possible communication graphs, where each graph $g = (V, E)$ represents a communication topology at a given time. The vertex set V corresponds to the agents \mathcal{N} , and the edge set E represents communication links. At each time step t , the current communication

¹This work adopts the convention that time step subscripts may be omitted when unambiguous. For instance, an action at time t for agent $i \in \mathcal{N}$ can be denoted explicitly as a_i^t or implicitly as a_i . Similarly, relative temporal notation is used, where s denotes the current state, a the selected joint action, and s' the successor state. This allows the reward function to be expressed compactly as $\mathcal{R}(s, a, s')$ instead of $\mathcal{R}(s^t, a^t, s^{t+1})$.

Table 1: Comparison of key related works in multi-agent exploration.

Ref	Name	Problem	Solution	MA
[17]	Self-Learn DRL	Unknown map exploration by finding the best sensing action.	DQL with and without RNNs. A CNN outputs the best sensing action from a local map and Frontier Rescue when the local map is completely known.	no
[9]	i-VFM	Reduce Multi Agent repetitive exploration	State representation (map), named i-VFM, that integrates the number of previous agent visits.	yes
[8]	MA Octomap	Autonomous exploration of unknown subterranean environments.	Navigation using a shared map with Graph-based and Frontier-based planning.	yes
[10]	Multi S-Graphs	Collaboratively and efficiently build a map with multiple agents.	Semantic Graphs.	yes

Abbreviations: MA - Multi-Agents.

graph² $g_t \in \mathbb{G}$ contains an edge (i, j) if and only if agents i and j can communicate at time t .

- $\gamma \in [0, 1]$ is the discount factor, determining the importance of future rewards.

Two primary approaches for solving these complex multi-agent problems are: (i) Formulating them as Distributed Constrained Optimization Problems (DCOPs), or (ii) Leveraging the structure of the communication graph using Graph Neural Networks (GNNs), which allow agents to efficiently aggregate and process information from their neighbors [20, 24, 21].

The approach proposed in this paper will not follow either of these options. It will simplify the problem by allowing neighboring agents to share observations. In this way, it avoids the computational complexity, whilst still benefitting from communication and coordination between agents.

3. Proposed Method

The implemented system architecture is comprised of two core components: the Godot-based environment simulation and the Python-based learning algorithm using Ray/RLlib, connected via the Godot RL Agents library, shown in Figure 1. The complete implementation is available in the GitHub repository [25].

3.1. Architecture

The Python-side implementation provides a foundation for large-scale experimentation:

- Single Trial: Configurable via a YAML file containing all hyperparameters (e.g., training batch size, number of agents, paradigm, etc.).

²The possible communication configurations grow exponentially with the number of agents $|\mathbb{G}| = 2^{\binom{n}{2}} = 2^{n(n-1)/2}$ for $n = |\mathcal{N}|$ agents.

- Multi-Trial: Leverage Ray’s distributed framework for parallel execution of grid searches, specific configurations, and hyperparameter tuning.
- Study: Preconfigured Multi-Trials.
- Hardware Abstraction: Ensures portability across HPC clusters (Deucalion and Cirrus) through environment detection and UV package management.
- Experiment Tracking: Weights & Biases [26] Integration for real-time monitoring of ~ 200 metrics per trial.

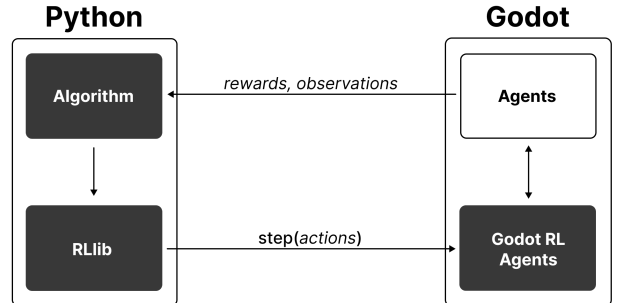


Figure 1: Godot-Python RL Process.

This complete architecture stack, illustrating both local and HPC execution paths, is summarized in Figure 2.

Environment Simulation is built using the Godot game engine [22], which provides a physically-grounded simulation with realistic constraints. With no loss of generality, the simulated UAV, controlled by the previously mentioned Python framework, is modeled after the DJI Tello. A comparison of the real-world UAV and its simulated counterpart is shown in Figures 3a and 3b.

With a simulation scale of $\frac{16\text{cm}}{80\text{px}} = 0.2\text{cm/px}$, the UAV Kinematics are also modeled after DJI Tello specifications with tuned velocities (0.8 m/s linear, 3 rad/s angular).

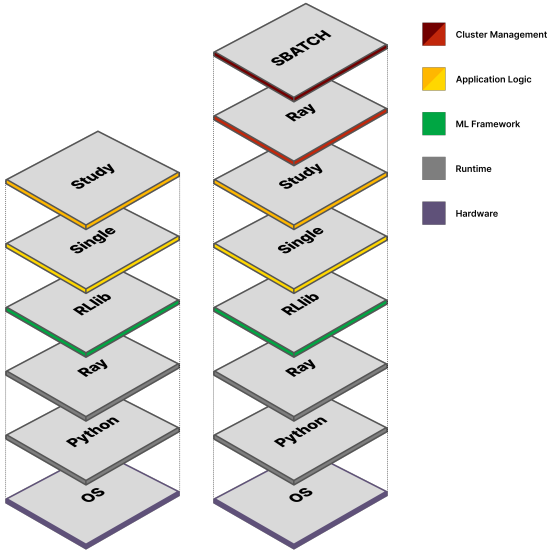


Figure 2: Architecture Stack.

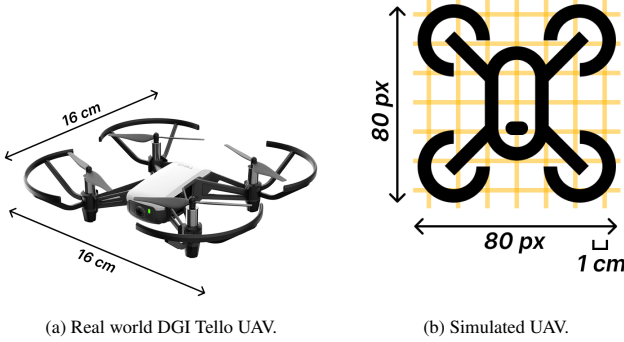


Figure 3: Real world UAV and its simulated counterpart.

It is assumed that the UAV model is equipped with a single sensor: a Light Detection and Ranging (LiDAR). The LiDAR is simulated using RayCast2D nodes with limited range and field of view. This information is used to update its *Local Map*, an Occupancy Grid Map, that utilizes Bayesian log-odds updates. The policy receives as input a fixed-size *Egocentric Map*, which is a portion of the *Local Map* centered on the agent. The integrated sensing and mapping pipeline is illustrated in Figure 4, showing LiDAR rays, color-modulated Local Map, and the Egocentric Map provided to policy networks.

The UAVs are capable of communicating using limited-range networking (depicted in Figure 5) with simulated transmission delays based on message size and bandwidth. They use a simple single-hop protocol, continuously share LiDAR data with agents in range, and share the entire *Local Map* upon (re)-establishing connection.

The modular Godot architecture, depicted in Figure 6, separates concerns through specialized managers for swarm control, communication, reward calculation, and logging.

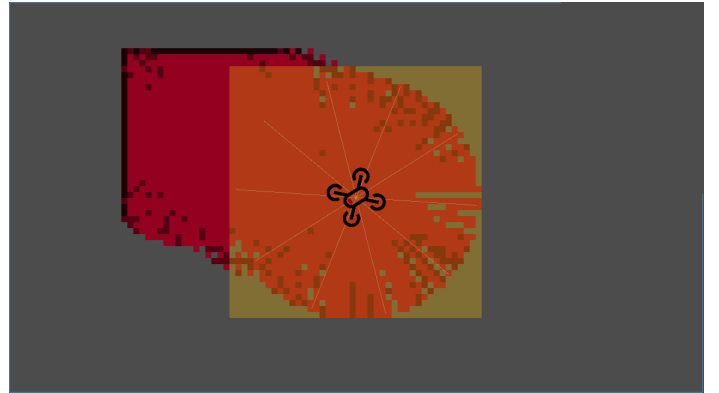


Figure 4: UAV sensing and mapping: (1) Simulated LiDAR rays (grey lines), (2) The Local Map of the agent (red area), and (3) The Egocentric Map provided to the policy network (yellow area).

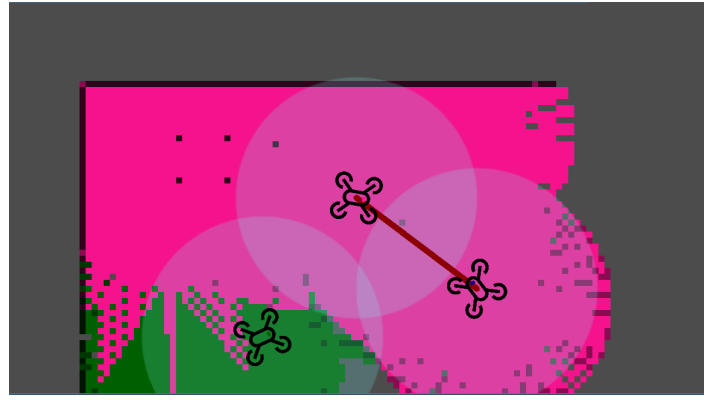


Figure 5: UAV network: communication ranges (blue circles), active links (red lines), and agent Local Maps (pink/green).

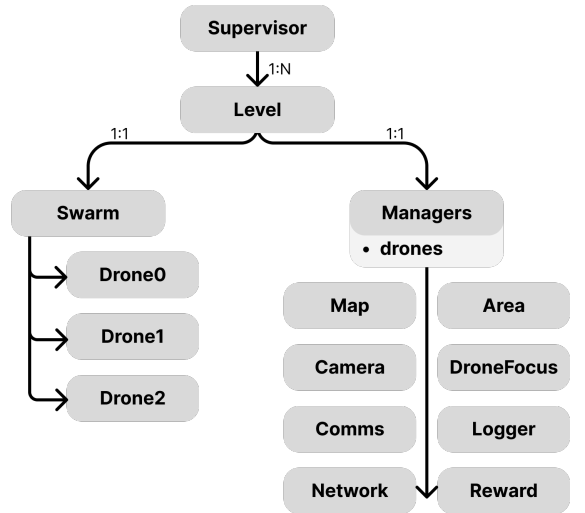


Figure 6: Godot Architecture.

MARL Paradigms Implementation. MARL paradigms are distinguished by their approach across two phases: training and execution. During training, the objective is to learn effective policies, typically with access to the global state. During execution, the goal is to deploy these trained policies in a decentralized, real-world setting without global state information. The three MARL paradigms [27] were implemented in the Godot-side to avoid RLLib modifications:

- Centralized Training Centralized Execution (CTCE) is a single agent solution to the multi-agent problem. All observations and actions are concatenated across agents, thus making it a non-scalable solution dependent on a centralized system for execution.
- Decentralized Training Decentralized Execution (DTDE): A fully decentralized approach where each agent trains and executes based on its own local observations. This paradigm offers high scalability and robustness [28] but often suffers from a lack of coordinated behavior among agents.
- Centralized Training Decentralized Execution (CTDE): A hybrid paradigm that leverages centralized information during training to learn more coordinated policies, which are executed in a decentralized manner. This approach aims to balance the training stability of centralized methods with the scalability of decentralized execution.

3.2. MARL Formulation

The multi-agent exploration problem is formalized as an ND-POMDP to account for partial observability and inter-agent communication. The framework is defined by the tuple $(\mathcal{N}, \mathbb{S}, \mathbb{A}, T, R, \mathbb{O}, O, \gamma, \mathbb{G})$, where homogeneous agents share identical action and observation spaces ($\mathbb{A}_i = \mathbb{A}_j, \mathbb{O}_i = \mathbb{O}_j$ for all $i, j \in \mathcal{N}$).

Reward Function. The primary objective is to maximize area coverage while avoiding redundant exploration. The reward function is designed to incentivize continuous discovery:

$$R(s, a, s') = W_{\text{area}} \cdot \Delta \text{Area}(s, s'), \quad (1)$$

where the coefficient W_{area} scales the area reward, and $\Delta \text{Area}(s, s')$ represents the new area discovered by the entire team during the state transition, normalized by the theoretical maximum discoverable area A_{max} per time step Δt . This normalization ensures stable learning and prevents gradient explosions.

In detail, $\text{Area}(s) = A_{\text{old}}$ and $\text{Area}(s') = A_{\text{new}}$ represent the total mapped area covered by the team before and after the state transition, respectively. The step-wise reward $R_{\text{step}} = R(s, a, s')$ is then calculated based on the normalized newly discovered area, defined as:

$$\Delta \text{Area}(s, s') = \frac{\text{Area}(s') - \text{Area}(s)}{A_{\text{max}}} = \frac{A_{\text{new}} - A_{\text{old}}}{A_{\text{max}}}, \quad (2)$$

The reward calculation, visualized in Figure 7, models sensor coverage as a circular field with radius r , equivalent to an ideal LiDAR with infinite rays. The theoretical maximum discoverable area per agent per time step, A_{max} , is calculated based on this coverage model and the maximum travel distance, given by $A_{\text{max}} = 2r \cdot v_{\text{max}} \Delta t$. The weighting coefficient W_{area} enables explicit trade-off calibration against other potential objectives (when used). For instance, if a collision penalty $R_{\text{collision}} = -1$ is introduced with weight $W_{\text{collision}}$, this quantitative trade-off is defined by the ratio $W_{\text{area}}/W_{\text{collision}}$. A configuration with $W_{\text{area}} = 1$ and $W_{\text{collision}} = 3$ implies an agent must discover 3 units of new area to compensate for a single collision.

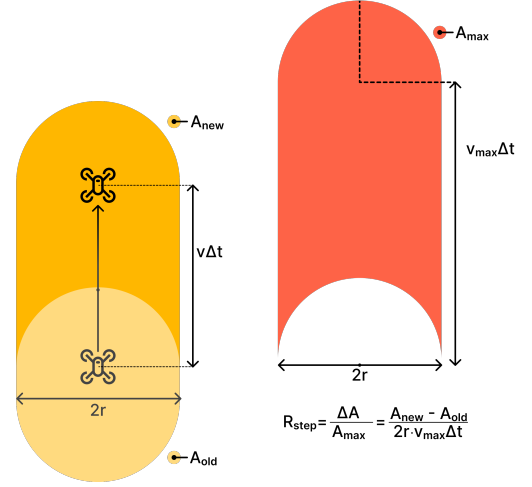


Figure 7: Reward per step.

Reward design proved critical in avoiding undesirable emergent behaviors. Early implementations with collision penalties led to the agents remaining stationary to avoid collisions. Rewarding only *newly discovered* area, rather than total accumulated area, effectively countered agent passivity and promoted continuous exploration. Poor exploration strategies are implicitly penalized through opportunity cost (reduced discovered area).

State. The system employs homogeneous agents with continuous action spaces to enable realistic UAV kinematics. The state $s \in \mathbb{S}$ comprises the complete 2D map environment, and the individual internal states of the agents characterized by: (i) position $p = (p_x, p_y)$ using x and y coordinates of the map m , (ii) rotation θ , (iii) linear velocity $v = (v_x, v_y)$, (iv) angular velocity ω . This is depicted in Figure 8.

Actions. The action space, defined in Equation (3), outputs normalized velocity commands:

$$a_i = (v_x, v_y, \omega) \in [-1, 1]^3 \quad (3)$$

These are scaled to realistic UAV velocities ($v_{\text{max}} = 400 \text{ px/s}$, $\omega_{\text{max}} = 3 \text{ rad/s}$). The continuous action space was chosen over

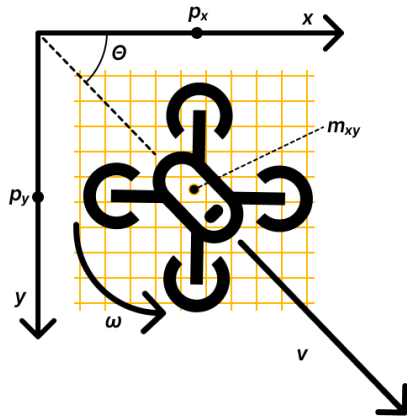


Figure 8: UAV State.

discrete alternatives to enable smooth trajectories and avoid exponential dimensionality growth, though it restricts the algorithm choice to policy-gradient methods like Proximal Policy Optimization (PPO).

Observations. Agents perceive their environment through a LiDAR sensor. The position and velocities of the agents are also considered observations. In a real-world scenario could originate from Global Navigation Satellite System (GNSS) (outdoor scenarios) and/or Integrated Navigation System (INS) [29]. This work utilizes perfect, noiseless observations from the simulation. This choice is intentional, as the focus is on MARL challenges rather than on perceptual noise robustness—in real world deployments this would be handled by off-the-shelf Simultaneous Localization And Mapping (SLAM) methods.

Furthermore, the communication protocol can provide agents with access to the LiDAR data and Local Maps of other agents. This information is used to update the agent's own Local Map.

Belief. The updated Local Map constitutes the belief of the agent about the environment. The belief of the agent, implemented as an Occupancy Grid Map (OGM), is updated in one of two ways. First, both self and shared LiDAR scans are incorporated using Bresenham's Line Algorithm to determine occupied and free cells. Second, shared Local Maps from other agents are fused by summing their log-odds probabilities³. Because the resulting Local Map is theoretically unbounded, the policy network receives a fixed-size Egocentric Map centered on the agent as its input.

Neural Network Architecture. Since PPO is an Actor-Critic algorithm, each agent employs two neural networks:

- Action policy (π_a): Maps the history to continuous actions.

³This is equivalent to a Bayesian update under the assumption of conditional independence. Given cell probabilities P_1 and P_2 from two maps, the fused probability is $P_c = \frac{P_1 P_2}{P_1 P_2 + (1-P_1)(1-P_2)}$, which corresponds to $L_1 + L_2$ in log-odds space. This assumption is valid as each UAV operates its own sensor.

- Value function (π_v): Estimates expected cumulative reward for the current state.

The Action-policy⁴ network architecture, illustrated in Figure 9, processes the spatially-structured Egocentric Map through a Convolutional Neural Network (CNN) while handling the LiDAR observation through a Fully-Connected layer. This hybrid architecture effectively combines spatial reasoning from the map with immediate sensory data from LiDAR. The policy's input and output configurations are modifiable. For example, the observation space can be extended to include inter-agent distances, and the action space can be reduced to pure 2D translation by excluding rotation.

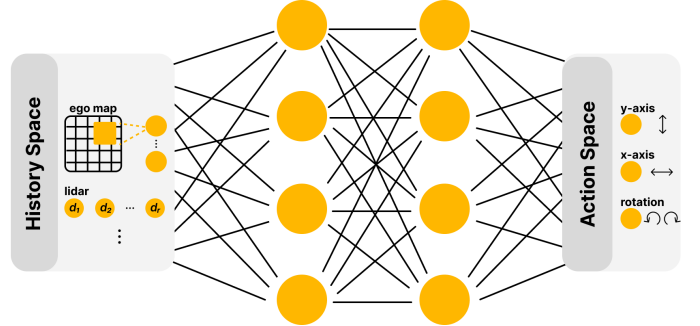


Figure 9: Action Policy Neural Network.

4. Results

To account for the inherent stochasticity of MARL, this work reports all environment-level metrics as the mean value over multiple episodes. This practice provides a more stable and robust performance estimate, with high values indicating that the policy is both high-performing and consistent.

4.1. Levels

Agents were tested across seven progressively complex environments (with increasing area and obstacles/rooms, shown in Figure 10) using all combinations of single/multi agent (1, 2, 3 agents), paradigms (CTCE, CTDE, DTDE), and specific levels (0-6). Each Trial consisting of 1000 Episodes of 1000 Steps.

All trials showed consistent reward improvement, with final discovered area summarized in Figure 11a. Performance increases from L0 to L4 but dips sharply at L5 (8.4%) due to obstacle-induced navigational challenges, before rising again at L6. This progression in difficulty is further illustrated in Figure 11b.

⁴The value-policy network π_v is not depicted, as it shares an identical structure except for the output layer, which consists of a single neuron representing the value estimate of the current state.

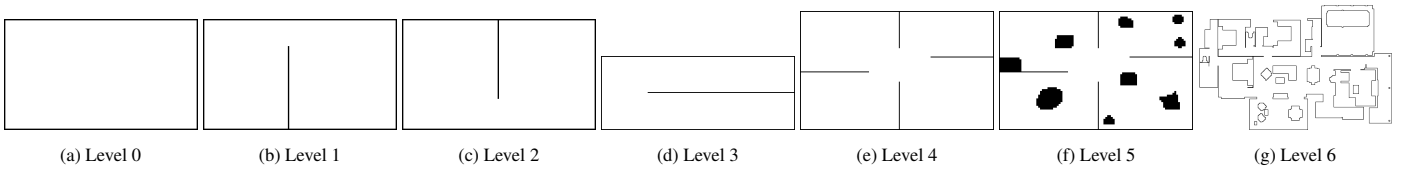
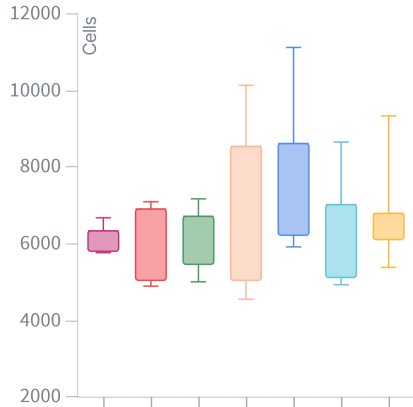
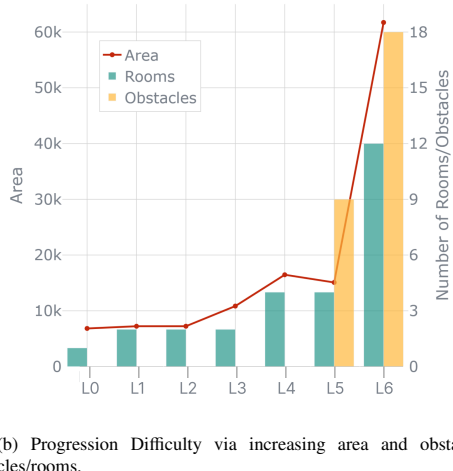


Figure 10: All Training Levels.

The policy loss demonstrates a consistent decrease, indicating continuous improvement throughout training, in Figure 12a. Additionally, the value function loss exhibits the expected pattern⁵ shown for Level 5 in Figure 12b, and is representative of all Levels. For improved clarity, Figures 12a and 12b utilize Exponential Weighted Average (EWMA) [30].



(a) Progression of level cells explored.



(b) Progression Difficulty via increasing area and obstacles/rooms.

Figure 11: Comparison of environment exploration and difficulty scaling.

⁵An initial rise followed by a decline. This occurs because as agents begin to learn and receive higher rewards, the value function must adapt to these new, higher value estimates, initially increasing the loss. Once learning stabilizes and rewards become more predictable, the value function converges to accurate state-value estimates, resulting in a decreasing loss.



Figure 12: Policy and Value Function Loss.

Key findings include the following:

- Scalability: Multi-agent configurations consistently outperformed single-agent setups, achieving up to 98% coverage in simpler levels (Figures 10a to 10c).
- Multi-Agent Complexity: 2-agent configurations occasionally outperformed 3-agent systems, demonstrating that the coordination complexity increases non-linearly with team size.
- Paradigms: CTCE, as a single-agent paradigm, greatly simplifies the problem, which accounts for its strong performance. However, CTDE emerged as the most effective training paradigm, particularly in complex environments where centralized value estimation provided advantages over the fully decentralized approach DTDE.
- Environmental Complexity: Performance naturally decreased with increasing obstacle density and exploration area, though absolute exploration capability improved as agents discovered more cells in larger environments.

Cross-level analysis (Figures 13a to 13c) confirm that higher

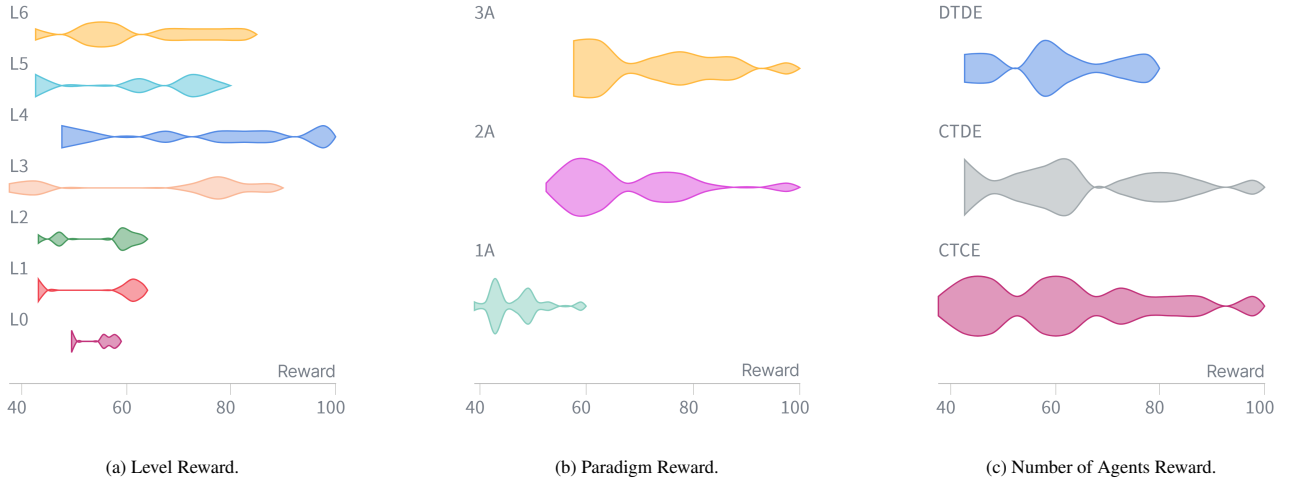


Figure 13: Reward per Level, Paradigm and Number of Agents.

agent counts yield superior results, and that the higher levels are more challenging, because of the gradual increase in reward range. Note that the higher levels are also larger, meaning a good navigating agent would gain a larger reward in the harder levels. This is evident for Level 6, the largest and most demanding, which has a large reward range with an even distribution.

4.2. Communication and Coordination

Analysis of inter-agent communication revealed significant collaborative benefits:

- Agents effectively shared environmental information, with communication accounting for up to 40% of discovered cells (as shown in Figure 14a).
- LiDAR Sharing proved more effective (responsible for 85% of shared cells declining to 60% over time) and more efficient than full Map Sharing⁶ (1% vs 99% of the bandwidth, as shown in Figure 14b), though both strategies contributed to exploration.
- Hypothetical emergent behaviors include both continuous motion coordination (maintaining proximity for LiDAR Sharing) or periodic regrouping for map synchronization.
- Cross-level analysis reveals bounded exploration and sharing dynamics: the ratios between agents remain within [0.5, 2]. This indicates that at any given time, one agent discovers at most twice as many cells as another, and similarly shares at most twice as many new cells.

⁶This inefficiency stems from transmitting the entire map rather than only discovered portions, and the absence of compression techniques such as Run-Length Encoding or LZMA2 (e.g., as used in 7zip).

To further quantify the effects of cooperation, team sizes of 2–4 agents were tested under the CTDE paradigm across three communication protocols: no communication (*off*), a constrained one-hop protocol (*one-hop*), and a multi-hop network (*multi-hop*) where messages are rebroadcast by all agents.

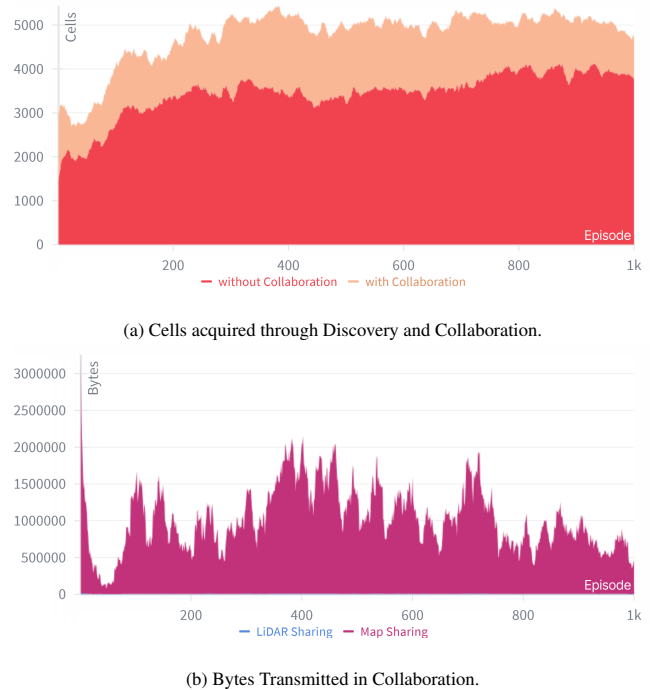


Figure 14: Cells from Discovery and Collaboration, and the Bytes Transmitted.

The results, presented in Figure 15, revealed a counterintuitive pattern: increased communication leads to worse overall performance.

It is hypothesized that this paradox arises because agents, through shared map information, learn to avoid areas marked as explored. In Level 4—which features a central chamber that must be traversed to access other rooms—this behavior becomes

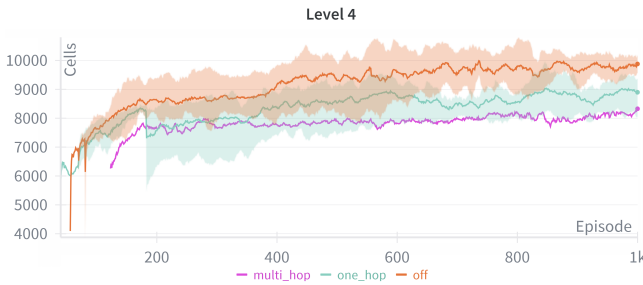


Figure 15: Performance across different communication protocols.

detrimental. If multiple agents learn to avoid this central area after initial exploration, they become trapped and unable to reach larger unexplored regions beyond it.

Thus, reducing communication limits shared map data, inadvertently helping agents identify unexplored areas. This further indicates that the current policy architecture lacks complexity required for navigating through a known area to reach unexplored regions.

4.3. Ablation Studies

Kill on Collision. This paper investigated variable-length episodes with early termination upon agent collisions, termed *Kill on Collision*, with the hypothesis that this would incentivize collision avoidance and improve navigation performance. Contrary to expectations, fixed-length episodes substantially outperformed this approach by a factor of 5.

Building on insights from single-agent formulations [18], a collision penalty $R_{\text{collision}} = -3$ was introduced. However, this resulted in the agents learning to become immobilized to avoid potential collisions.

These findings highlight that MARL formulations present substantially greater complexity than single-agent scenarios, requiring careful consideration of reward structures and termination conditions to avoid unintended behaviors.

Parallel vs Sequential. Given the hierarchical structure of the environment levels⁷, two Curriculum-Learning strategies were evaluated: (i) Parallel training on all levels simultaneously, and (ii) Sequential training, where agents progress through levels one-by-one (upon reaching 80% area coverage).

Sequential progression proved more effective, achieving a 250% higher performance than the Parallel strategy. This result is attributed to *catastrophic interference* in the Parallel setting,

where the diverse and conflicting dynamics from all levels simultaneously overwhelm the policies of the agents, preventing stable learning. In contrast, the Sequential curriculum allows the agent to construct knowledge incrementally, mastering fundamental skills in earlier levels that robustly transfer to more complex ones.

Curriculum-Learning. A key limitation of the previous Sequential training was the overly simplistic passing condition. Requiring 80% area coverage to be achieved only once could result from policy exploration rather than demonstrating a consistent ability.

Parametrizing via `pass_area` (coverage threshold) and `pass_x_times` (consistency requirement), for example, reaching 80% area 20 times, allowed this Curriculum-Learning formulation to enhance performance, and speed up training.

Figure 16 illustrates `pass_area` varying between 60, 70, 80 and 90% and `pass_x_times` varying between 1, 10, 15 and 20. Level 3 revealed clear interactions between threshold difficulty and required consistency.



Figure 16: Level 3.

Figure 16 shows varying intervals resulting from changing passing conditions. Several key behaviours were identified:

- (1) Harder progression criteria enhance learning, the **80% (20x)** demonstrates immediate performance advantages over **80% (15x)**, which in turn outperforms **60% (20x)**. likewise the **90% (15x)>(10x)>(1x)**, confirming a positive correlation between progression difficulty and learning effectiveness.
- (2) Reliability Over Early Success: The **90% (1x)** condition advances to Level 3 approximately 50 episodes earlier than **80% (20x)**, yet the latter achieves immediately superior performance. The single-success condition shows only gradual improvement and remains consistently dominated by multi-success variants (**15x**, **10x**), validating the emphasis on *reliable* performance over episodic luck.
- (3) Perfectionism: Excessively high coverage thresholds (**90%**) with variants (**15x**), (**10x**), and (**1x**) achieve lower overall performance than **80% (20x)**. Reaching the higher

⁷The levels monotonically increase in explorable area and obstacle density. Level 1 introduces basic walls, Level 3 adds obstacles, Level 4 expands the scale with more rooms, Level 5 increases obstacle density, and Level 6 serves as the most realistic and complex scenario, created using a house blueprint.

90-100% coverage rates proves very challenging, because of the mapping gaps during movement and the possible need for backtracking through discovered area to locate small remaining gaps.

(4) Balance: The **80% (20x)** condition achieves an area mean of 80%, suggesting that these hyperparameters may represent an optimal balance, enforcing consistent performance without excessive perfectionism.

4.4. Optimizing Actions and Observations

The policies of the agents exhibited significant sensitivity to the formulation of both actions and observations. A grid search over these design possibilities revealed clear performance hierarchies.

When grouping by action space, a consistent ranking emerged: movement in a 2D plane without rotation outperformed 1D movement with independent rotation, both of which substantially surpassed a waypoint-based approach where the agent specifies a target direction and the drone automatically rotates and moves⁸.

Analysis by observation space showed less pronounced differentiation, though trendlines consistently favored the combination of the Egocentric Map with LiDAR data. The explicit inclusion of inter-agent distances proved detrimental to learning efficiency. It is hypothesized that LiDAR measurements already implicitly encode proximity information, albeit without distinguishing between agent and obstacle contacts. Meanwhile, LiDAR-only observation proved insufficient, aligning with expectations since only the Egocentric Map incorporates historical observations, providing the essential temporal context for effective navigation.

4.5. Architectural Optimizations

Several neural network enhancements significantly improved performance.

Centralized Critic. Parameter sharing across value functions provided a small improvement (1% area coverage).

LiDAR Convolutions. 1D CNN processing of LiDAR data increased performance by 20%, allowing agents to overcome previous performance barriers and advance to the more complex Level 5 (Figure 17a). Two different convolution filters were tested: a single and a double layer one, with the deeper layered one showing better performance.

⁸Manual control in this mode proved challenging and unintuitive, warranting further refinement. Such control mechanisms resemble two-stage RL formulations, introducing additional learning complexity that conflicts with the end-to-end approach utilized by this work.

RNN Integration. Temporal processing improved performance (13%), with optimal configurations combining LiDAR and global positioning data (Figure 17b), though at the cost of slower training convergence. The baseline achieved comparable cell discovery within 70 episodes, while the RNN approach required 220 episodes to surpass this threshold.

The best performing configurations used global positioning data. This enables agents to learn panning motions for systematic area coverage by leveraging temporal sequences of global positions. Furthermore, by analyzing position history, agents can reason about unexplored regions, raising questions about global versus local planning strategies. The current formulation optimizes for local exploration by incentivizing immediate area discovery, whereas a global approach might initially target less rewarding areas to minimize future backtracking. Global planning approaches are more aligned with the objective of achieving complete area coverage (90-100%), which represents a related problem, but beyond the scope of this work.

The inferior performance of RNNs with only LiDAR observations, compared to the belief-based approach without RNNs presented in this work (the Egocentric Map), demonstrates that the indiscriminate application of RNNs—as commonly employed in other works to address partial observability—can be suboptimal. As explained in Section 2, RNNs will implicitly construct belief states from the LiDAR data, functionally similar to the explicit map representation in *ego_map*. However, the explicit map offers superior interpretability and enables straightforward inter-agent communication through map merging. By contrast, the latent space of RNNs lacks inheritance

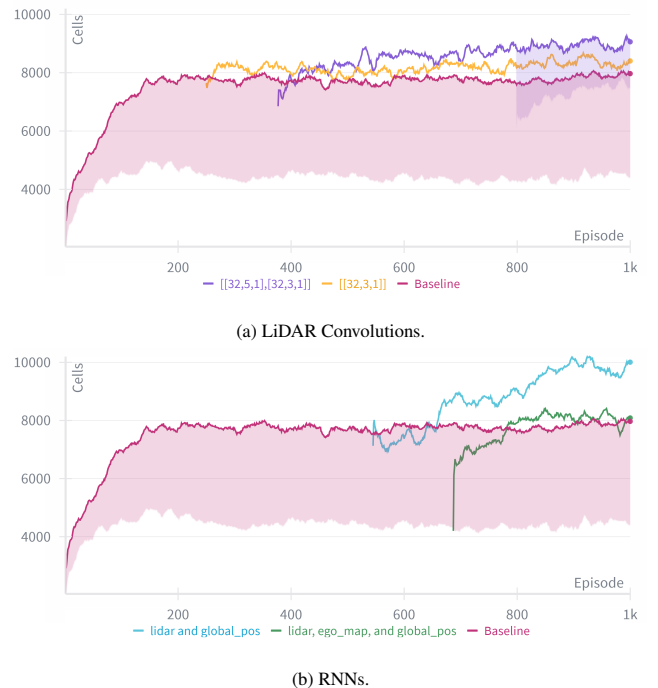


Figure 17: Architectural optimizations in Level 5: (a) convolutional processing of LiDAR data or (b) the integration of RNNs for temporal reasoning.

ent interpretability, and merging these representations between agents presents significant challenges.

5. Conclusions

This work presents a framework for multi-agent communication-aware exploration of unknown indoor environments. A decentralized and scalable multi-agent system is considered within a constrained communication network to approximate real mission conditions.

The capabilities of the framework are demonstrated through the application of MARL to train a group of UAVs to collaboratively explore an unknown GNSS-denied indoor environment using high-fidelity game-engine simulation. Each UAV agent is equipped with a LiDAR sensor, which is used to build a local occupancy map. Each agent can also exchange data with neighbouring agents in a limited range. UAV agents are trained in continuous action spaces to navigate under uncertainty using ND-POMDPs.

Through extensive ablation studies, this work systematically evaluates key factors, including training paradigms, reward functions, and network architectures. It also demonstrates that Curriculum-Learning significantly accelerates and stabilises training. Furthermore, the resulting policies address critical limitations of prior work, such as reliance on discrete actions and centralized control, thereby laying a principled foundation for deploying learned strategies onto physical robotic systems.

Experimental results yield several key findings:

- (1) A multi-agent perspective is essential. For instance, penalty-based collision avoidance resulted in agents learning not to move.
- (2) A SLAM-RL integration proved to be more effective than standard RNNs for handling partial observability.
- (3) A specialized LiDAR convolution network provided a 20% performance gain, underscoring the value of domain-specific perception architectures.
- (4) A robust and accessible simulation framework was established using the Godot Engine, providing a lightweight, open-source platform with high-fidelity physics, validated with industry-grade tools on an HPC cluster.
- (5) Training was successfully achieved via a structured Curriculum-Learning approach, enabling agents to master navigation in progressively complex environments.

The work acknowledges inherent limitations, including the substantial sample complexity of MARL, which required extensive training durations, and potential challenges in environment generalization. Furthermore, the study focuses on a comparison of

multi-agent learning paradigms rather than direct benchmarks against classical coverage algorithms (e.g. frontier-based).

Positioned as a stepping stone for future work, the research outlines a comprehensive trajectory for subsequent investigation. Prospective directions include the following:

- **Improved sensors and observations**, including visual sensors and Visual-SLAM support, dynamic rotation within the egocentric map for smoother UAV trajectories [18], and limiting the LiDAR field-of-view from the unrealistic 360°.
- **Expansion to 3D** settings, adapting the formulations of agent kinematics, accounting for different information gains from observations and resulting beliefs, as well as the impact of communication limitations in mission performance.
- **SLAM-RL**. Experiment with different options, leveraging the commonalities, for instance Graph-SLAM and GNNs on the RL side.
- **Enhanced agent models and learning algorithms**, including improved credit assignment via value decomposition (e.g., Q-value Mixing (QMIX) [31]); hierarchical policies for multi-level decision-making; pre-training through imitation learning from expert demonstrations; competitive dynamics via game-theoretic self-play [32]; and integrated planning with AlphaZero-inspired search algorithms such as Monte Carlo Tree Search.
- **Temporal reasoning**. The performance improvement observed when applying RNNs to *ego_map* likely stems from temporal reasoning about agent movement patterns, analogous to frame stacking in RL. This could be done by applying 3D CNNs.

Given these considerations, the formulation with LiDAR Convolutions may be preferable due to its applicability to GNSS-denied environments, architectural simplicity, and faster training despite the 12.5% reduction in final performance compared to the best RNN configuration. Future research on improved observation representations could further narrow this performance gap.

Acknowledgements

The author wishes to thank HPCvLAB, whose computational resources made this work possible in its current form. Providing access to the Deucalion [33] and Cirrus [34] HPC Clusters.

This work is supported by the Portuguese Foundation for Science and Technology (FCT) under Grant 2023.04842.BD.

This work is also funded by national funds through FCT – Fundação para a Ciência e a Tecnologia, I.P., under

projects/supports UID/6486/2025 (<https://doi.org/10.54499/UID/6486/2025>) and UID/PRR/6486/2025 (<https://doi.org/10.54499/UID/PRR/6486/2025>).

References

[1] H. A. Foudeh, P. C.-K. Luk, J. F. Whidborne, An advanced unmanned aerial vehicle (uav) approach via learning-based control for overhead power line monitoring: A comprehensive review, *IEEE Access* 9 (2021) 130410–130433. doi:10.1109/ACCESS.2021.3110159.

[2] N. Boonyathanmig, S. Gongmanee, P. Kayunyeam, P. Wutticho, S. Prongnuch, Design and implementation of mini-uav for indoor surveillance, in: 2021 9th International Electrical Engineering Congress (iEECON), 2021, pp. 305–308. doi:10.1109/iEECON51072.2021.9440350.

[3] I. Mademlis, V. Mygdalis, N. Nikolaidis, M. Montagnuolo, F. Negro, A. Messina, I. Pitas, High-level multiple-uav cinematography tools for covering outdoor events, *IEEE Transactions on Broadcasting* 65 (3) (2019) 627–635. doi:10.1109/TBC.2019.2892585.

[4] D. Rakesh, N. Akshay Kumar, M. Sivaguru, K. V. R. Keerthivaasan, B. Rohini Janaki, R. Raffik, Role of uavs in innovating agriculture with future applications: A review, in: 2021 International Conference on Advancements in Electrical, Electronics, Communication, Computing and Automation (ICAEECA), 2021, pp. 1–6. doi:10.1109/ICAEECA52838.2021.9675612.

[5] J. Dong, K. Ota, M. Dong, Uav-based real-time survivor detection system in post-disaster search and rescue operations, *IEEE Journal on Miniaturization for Air and Space Systems* 2 (4) (2021) 209–219. doi:10.1109/JMASS.2021.3083659.

[6] Emerging and Cross-cutting Aviation Issues 2014; Increased use of unmanned aircraft systems (UAS) — icao.int, <https://www.icao.int/annual-report-2021/Pages/emerging-and-cross-cutting-aviation-issues-increased-use-of-unmanned-aircraft-systems-uas.aspx>, [Accessed 12-01-2025].

[7] B. Yamauchi, A frontier-based approach for autonomous exploration, in: Proceedings 1997 IEEE International Symposium on Computational Intelligence in Robotics and Automation CIRA'97. 'Towards New Computational Principles for Robotics and Automation', 1997, pp. 146–151. doi:10.1109/CIRA.1997.613851.

[8] M. T. Ohradzansky, E. R. Rush, D. G. Riley, A. B. Mills, S. Ahmad, S. McGuire, H. Biggie, K. Harlow, M. J. Miles, E. W. Frew, C. Heckman, J. S. Humbert, Multi-agent autonomy: Advancements and challenges in subterranean exploration (2021). arXiv:2110.04390. URL <https://arxiv.org/abs/2110.04390>

[9] X. Chen, A. N. Iyer, Z. Wang, A. H. Qureshi, Efficient q-learning over visit frequency maps for multi-agent exploration of unknown environments (2023). arXiv:2307.16318. URL <https://arxiv.org/abs/2307.16318>

[10] M. Fernandez-Cortizas, H. Bavle, D. Perez-Saura, J. L. Sanchez-Lopez, P. Campoy, H. Voos, Multi s-graphs: An efficient distributed semantic-relational collaborative slam, *IEEE Robotics and Automation Letters* 9 (6) (2024) 6004–6011. doi:10.1109/LRA.2024.3399997. URL <http://dx.doi.org/10.1109/LRA.2024.3399997>

[11] H. Choset, P. Pignon, Coverage path planning: The boustrophedon cellular decomposition, in: A. Zelinsky (Ed.), *Field and Service Robotics*, Springer London, London, 1998, pp. 203–209.

[12] J. Wang, R. Wang, Multi-uav area coverage track planning based on the voronoi graph and attention mechanism, *Applied Sciences* 14 (17) (2024). doi:10.3390/app14177844. URL <https://www.mdpi.com/2076-3417/14/17/7844>

[13] E. U. Acar, H. Choset, A. A. Rizzi, P. N. Atkar, D. Hull, Morse decompositions for coverage tasks, *The International Journal of Robotics Research* 21 (2002) 331 – 344. URL <https://api.semanticscholar.org/CorpusID:12656982>

[14] S. Karaman, E. Frazzoli, Sampling-based algorithms for optimal motion planning (2011). arXiv:1105.1186. URL <https://arxiv.org/abs/1105.1186>

[15] Z. Shen, J. P. Wilson, S. Gupta, C*: A coverage path planning algorithm for unknown environments using rapidly covering graphs (2025). arXiv: 2505.13782. URL <https://arxiv.org/abs/2505.13782>

[16] X. Chen, T. M. Tucker, T. R. Kurfess, R. Vuduc, Adaptive deep path: Efficient coverage of a known environment under various configurations, in: 2019 IEEE/RSJ International Conference on Intelligent Robots and Systems (IROS), IEEE Press, 2019, p. 3549–3556. doi:10.1109/IROS40897.2019.8967793. URL <https://doi.org/10.1109/IROS40897.2019.8967793>

[17] F. Chen, S. Bai, T. Shan, B. Englot, Self-learning exploration and mapping for mobile robots via deep reinforcement learning, *AIAA Scitech 2019 Forum* (2019). URL <https://api.semanticscholar.org/CorpusID:68149666>

[18] A. Jonnarth, J. Zhao, M. Felsberg, Learning coverage paths in unknown environments with deep reinforcement learning (2024). arXiv:2306.16978. URL <https://arxiv.org/abs/2306.16978>

[19] C. Guestrin, D. Koller, R. E. Parr, Multiagent planning with factored mdps, in: *Neural Information Processing Systems*, 2001. URL <https://api.semanticscholar.org/CorpusID:6487585>

[20] Z. Liu, J. Zhang, E. Shi, Z. Liu, D. Niyato, B. Ai, Xuemin, Shen, Graph neural network meets multi-agent reinforcement learning: Fundamentals, applications, and future directions (2024). arXiv:2404.04898. URL <https://arxiv.org/abs/2404.04898>

[21] C. Sun, M. Shen, J. P. How, Scaling up multiagent reinforcement learning for robotic systems: Learn an adaptive sparse communication graph (2020). arXiv:2003.01040. URL <https://arxiv.org/abs/2003.01040>

[22] G. Engine, Godot Engine - Free and open source 2D and 3D game engine — godotengine.org, <https://godotengine.org/>, [Accessed 02-12-2024].

[23] F. Oliehoek, C. Amato, A Concise Introduction to Decentralized POMDPs, *SpringerBriefs in Intelligent Systems*, Springer International Publishing, 2016. URL <https://books.google.pt/books?id=FZRPDAAQBAJ>

[24] A. Goeckner, Y. Sui, N. Martinet, X. Li, Q. Zhu, Graph neural network-based multi-agent reinforcement learning for resilient distributed coordination of multi-robot systems (2024). arXiv:2403.13093. URL <https://arxiv.org/abs/2403.13093>

[25] T. Leite, GitHub - TiagoMLEite/IMAGINE — github.com, <https://github.com/TiagoMLEite/IMAGINE> (2025).

[26] wandb.ai, <https://wandb.ai/site/>, [Accessed 16-10-2025].

[27] Z. Ning, L. Xie, A survey on multi-agent reinforcement learning and its application, *Journal of Automation and Intelligence* 3 (2) (2024) 73–91. doi:<https://doi.org/10.1016/j.jai.2024.02.003>. URL <https://www.sciencedirect.com/science/article/pii/S294955424000042>

[28] K. Zhang, Z. Yang, H. Liu, T. Zhang, T. Başar, Fully decentralized multi-agent reinforcement learning with networked agents (2018). arXiv: 1802.08757. URL <https://arxiv.org/abs/1802.08757>

[29] Autonomous Navigation & Positioning for Drones, UAV, UGV, USV & AUV — unmannedsystemstechnology.com, <https://www.unmannedsystemstechnology.com/expo/autonomous-navigation/>, [Accessed 11-01-2025].

[30] Exponentially Weighted Moving Average (EWMA) — corporatefinance-institute.com, <https://corporatefinanceinstitute.com/resources/career-map/sell-side/capital-markets/exponentially-weighted-moving-average-ewma/>, [Accessed 16-10-2025].

[31] T. Rashid, M. Samvelyan, C. S. de Witt, G. Farquhar, J. Foerster, S. Whiteson, Qmix: Monotonic value function factorisation for deep multi-agent reinforcement learning (2018). arXiv:1803.11485. URL <https://arxiv.org/abs/1803.11485>

[32] R. Zhang, Z. Xu, C. Ma, C. Yu, W.-W. Tu, S. Huang, D. Ye, W. Ding, Y. Yang, Y. Wang, A survey on self-play methods in reinforcement learning (2024). arXiv:2408.01072. URL <https://arxiv.org/abs/2408.01072>

[33] MACC, Deucalion - Deucalion User Guide — docs.macc.fccn.pt, <https://docs.macc.fccn.pt/deucalion/>, [Accessed 04-10-2025].

[34] INCD-Lisbon (cirrus.a.... | INCD user documentation — wiki.incd.pt, <https://wiki.incd.pt/books/compute-node-specs-and-information>, [Accessed 04-10-2025].